Available online at www.sciencedirect.com
ScienceDirect
Trans. Nonferrous Met. Soc. China 25(2015) 1811−1821
Transactions of Nonferrous Metals Society of China
www.tnmsc.cn

Effect of complex melt-refining treatment on microstructure and mechanical properties of sand-cast Mg–10Gd–3Y–0.5Zr alloy

Jun MEI[1], Wen-cai LIU[1,2], Guo-hua WU[1], Yang ZHANG[1], Yi-tao ZHANG[1], Yi-kai HONG[1], Ruo-xi ZHANG[1], LÜ XIAO[3], Wen-jiang DING[1]

1. National Engineering Research Center of Light Alloys Net Forming and State Key Laboratory of Metal Matrix Composite, Shanghai Jiao Tong University, Shanghai 200240, China;
2. Shanghai Light Alloy Net Forming National Engineering Research Center Co., Ltd., Shanghai 201615, China;
3. Shanghai Aviation Precision Machinery Research Institute, Shanghai 201600, China

Received 2 July 2014; accepted 17 October 2014

Abstract: The effect of complex melt-refining treatment (melt flux incorporating with rotating gas bubble stirring) on microstructure and mechanical behavior of the sand-cast Mg−10Gd−3Y−0.5Zr alloy was investigated. In addition, the melt purifying mechanism of the complex melt-refining treatment for the sand-cast alloy was discussed systematically. The results show that the new melt-refining method can significantly improve melt quality and mechanical behavior of the tested alloy, i.e., compared to the reference unpurified alloy, the volume fraction of inclusions decreased from 0.47% to 0.28%, the ultimate tensile strength and elongation for T6-treated alloy increased from 245 MPa and 0.7% to 312 MPa and 4.5%, respectively. Especially, combining 1% flux with rotating gas bubble stirring can get even better purifying effectiveness than conventional sole 2% flux purification; the use of melt flux decreased by 50% and significantly reduced environmental pollution.

Key words: magnesium alloy; sand-cast; purification; complex melt-refining; mechanical property

1 Introduction

It has been demonstrated that rare earth can significantly improve the strength, heat and corrosion resistance of the conventional magnesium alloys [1,2], which makes the rare-earth magnesium alloys (Mg–RE) more and more attractive for aerospace and automotive applications. Among different kinds of Mg–RE alloys, Mg−Gd−Y system is one of the most promising candidates due to its high specific strength at both room and elevated temperatures, and better creep resistance than other Mg−RE alloys [3−5]. In the past few years, a number of investigations related to the microstructure and mechanical properties of the Mg−Gd−Y system formed in metal mould have been reported. ANYANWU et al [4] and MIRZA et al [5] investigated the relationship between mechanical properties and microstructure of Mg−Gd−Y alloys. HE et al [6] observed the precipitation sequence of Mg−Gd−Y alloy during isothermal aging at 250 °C for 0−2400 h. Recently, CHANG et al [7] have investigated the effect of different Gd contents on the corrosion behavior of Mg−Gd−Y alloys. WANG et al [8] investigated the effect of Y on enhanced age hardening response and mechanical properties of Mg−Gd−Y alloys. HONMA et al [9] investigated the effect of Zn additions on the remarkable age-hardening and unusual plastic elongation behaviors of Mg−Gd−Y alloys. Given the results in literatures [4−9], the Mg−10Gd−3Y−0.5Zr alloy exhibits higher strength and better ductility compared with other Mg−Gd−Y alloys.

However, owing to the high chemical activity of both magnesium and rare earth elements, they tend to oxidize rapidly and burn in air to bring a lot of inclusions into the Mg melt during the alloy melting process [10]. It is known that inclusions can destroy the continuity of the magnesium matrix and thus significantly reduce the comprehensive properties of the Mg−RE alloys as the cradle of defects such as pores and cracks [11,12]. Now

Foundation item: Project (USCAST2012-15) supported by the SAST-SJTU Joint Research Centre of Advanced Aerospace Technology; Project (B type, 14QB1403200) supported by the Shanghai Rising-Star Program, China; Projects (20120073120011, 20130073110052) supported by the Research Fund for the Doctoral Program of Higher Education of China; Project (IPP9084) supported by IPP program in SJTU, China
Corresponding author: Wen-cai LIU; Tel: +86-21-54742630; Fax: +86-21-34202794; E-mail: liuwc@sjtu.edu.cn
DOI: 10.1016/S1003-6326(15)63787-6

the purification technology of Mg−RE alloy has become one of the key bottlenecks which restrict its application in industry. Therefore, the study on refining technologies for further improving the inherent quality of Mg−RE alloys has practical significance.

The conventional flux purification has always been considered the most effective purifying method because of its favorable refining ability and easy operation. However, to get the expected effects, the amount of fluxes is at least 2% (mass fraction) which results in severe environmental pollution and may increase the chance of additional flux inclusions. Sometimes large flux inclusions get trapped in the magnesium, causing deterioration of certain mechanical properties. Therefore, the traditional flux-based refining techniques are not the optimal solution for magnesium melt purification. Recently, the gas bubbling as a non-flux refining method has attracted more and more attention due to its inclusion removing ability and excellent degassing capacity [13,14]. However, up to now, no researches on the effect of flux incorporating with gas bubbling refining process on the microstructure and mechanical properties of Mg−RE alloys were reported. In this work, the effect of JDMJ flux incorporating with gas bubbling purification on the microstructure and mechanical properties of sand-cast Mg−10Gd−3Y−0.5Zr alloy was investigated, aiming to optimize as well as improve the efficiency of traditional flux refining treatment.

2 Experimental

2.1 Smelting and refining process

The material used in this work is Mg−10Gd−3Y−0.5Zr (named as GW103K, mass fraction, %) alloy, which can be produced by sand mould casting. Mg−90Gd and Mg−25Y (mass fraction, %) master alloys were made first by melting high-purity elemental Mg (>99.95%), Gd (>99.9%) and Y (>99.9%) in a vacuum medium-frequency induction furnace under an argon atmosphere. The alloying process with a nominal composition of Mg−10Gd−3Y−0.5Zr was then prepared from high-purity Mg (99.95%), the Mg−90Gd, Mg−25Y and Mg−30Zr master alloys in a 7 kW electric resistance furnace under the mixed atmosphere of CO_2 and SF_6 with the volume ratio of 100:1 [15]. The components of JDMJ flux are listed in Table 1. The total mass of the raw metal was 8 kg per charge. The JDMJ fluxes of 0, 1%, 2% (mass fraction, %) were then employed to refine the melt at 740 °C, at the same time, a rotary impeller [16] was inserted into the melt and then an inert gas, Ar, was introduced through the impeller hole, the size of which was 0.2 mm in diameter. The rotating speed was 150 r/min, the gas flow rate was 2 L/min and the refining process lasted for 10 min, which is the optimal parameter combination according to the early stage of our study. During the whole refining procedure, the temperature was controlled at (740±10) °C by an electrothermal couple immersed in the melt directly and the mixed protecting gas atmosphere discussed before is also indispensable.

Table 1 Components of JDMJ flux (mass fraction, %)

$MgCl_2$	KCl	NaCl	$BaCl_2$	$CaCl_2$	CaF_2
40−50	15−25	15−20	3−5	3−5	5−10

After refining treatment, the melt was held for 25−40 min, and then, at 720 °C, cast in sand mould of 130 mm × 250 mm block shape (see Fig. 1) which was made by precoated sand. The real chemical composition was determined to be Mg−10.18Gd−2.85Y−0.42Zr by an inductively coupled plasma analyzer (ICP, Perkin Elmer, Plasma–400).

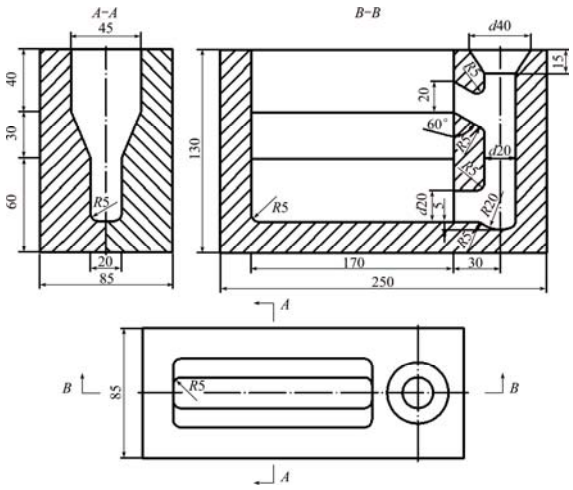

Fig. 1 Schematic diagram of casting mold (unit: mm)

2.2 Properties test

Based on the experimental results in the Ref. [17], T6 heat treatment (solution treatment followed by artificial aging (525 °C, 12 h+ 250 °C, 10 h)) was applied to these cast ingots, and the sample was named as sand-cast-T6. Sheet tensile samples of 3.5 mm in width, 2 mm in thickness, and 10 mm in gauge length were cut from the casting ingots by the electric-sparking wire-cutting machine. Tensile properties of the tested alloys were performed at the initial strain rate of 5×10^{-4} s^{-1} referred to the ASTM: E8M−13a standard on Zwick/Roell Z020 tensile machine at room temperature.

Statistical volume fractions of nonmetallic inclusions in alloys were measured with Image-Pro Plus software. Phase composition was scanned by a Rigaku Dmax-rc X-ray diffractometer (XRD) using Ni-filtered Cu K_α radiation. The microstructures, chemical composition analysis, and tensile fracture surfaces of the

investigated alloys were observed by using optical microscope (OM) and scanning electron microscope (SEM, Philips 505, Holland), respectively.

3 Results

3.1 Effect of complex purification treatment on microstructures and non-metallic inclusions

Five different purification conditions are chosen to study the effect of JDMJ flux incorporating with rotating gas bubble stirring refining process (Table 2). Figure 2 shows the microstructures of the unrefined, gas bubbling and complex method refined sand-cast GW103K alloys. WANG et al [18] has demonstrated that the black spots in the figures are non-metallic inclusions which consist mainly of MgO and oxides of Gd and Y. It is clear that compared to the unrefined alloy in Fig. 2(a), the inclusions are reduced after rotating gas bubbling process (Fig. 2(c)). When the new complex treatment was employed, the amount of inclusions is further reduced and clean melt can be achieved as shown in Fig. 2(e). The corresponding XRD analysis results are presented in Fig. 3, which suggests that the microstructures (Figs. 2(b), (d) and (f)) of the sand-cast GW103K alloy after purification still consist of equiaxed α(Mg) matrix and network eutectic compounds ($Mg_{24}(Gd,Y)_5$) distributing at grain boundaries.

As seen in Fig. 4, after T6 treatment, all the eutectic phases dissolved into the matrix. Figures 4(a) and (c) show the microstructures of the sand-cast-T6 GW103K

Table 2 Five different purifying treatments

Treatment method No.	Purifying treatment
I	Unpurified
II	Gas bubbling purifying
III	2% JDMJ flux purifying
IV	1% JDMJ flux + gas bubbling
V	2% JDMJ flux + gas bubbling

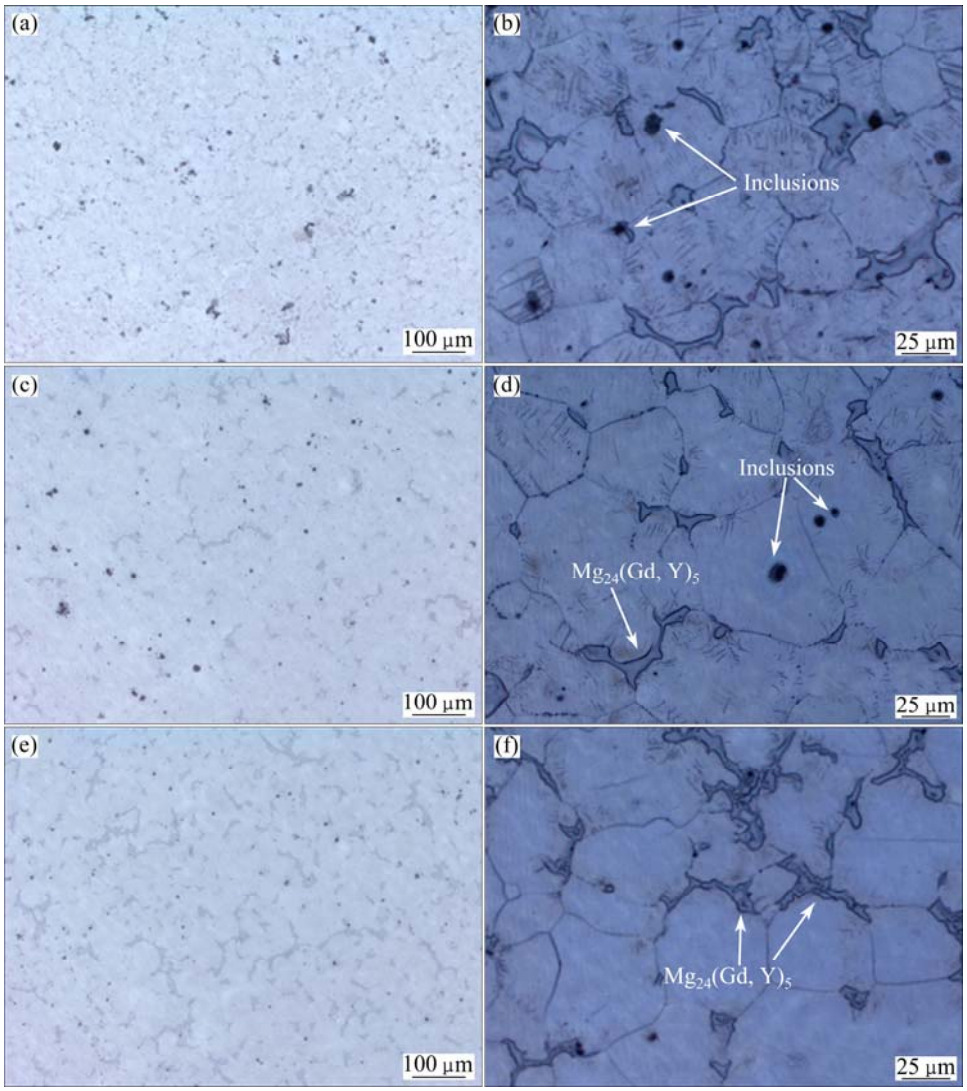

Fig. 2 Microstructures of sand-cast GW103K alloy purified by different treatments: (a) Unpurified; (b) Magnified view of (a); (c) Gas bubbling; (d) Magnified view of (c); (e) 1% JDMJ flux +gas bubbling; (f) Magnified view of (e)

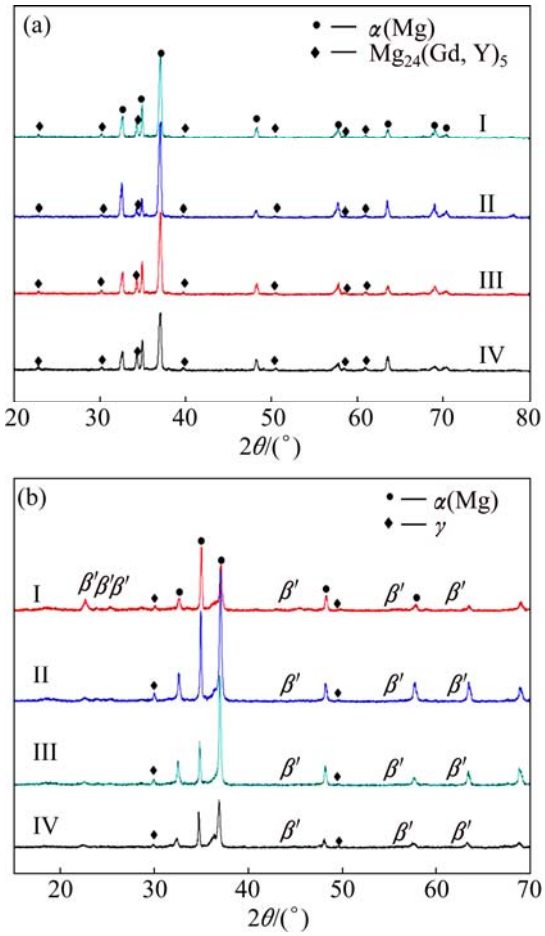

Fig. 3 XRD patterns of sand-cast (a) and sand-cast-T6 (b) GW103K alloys under different purifying treatments

alloys before and after combined purification, respectively. It is observed that the cluster inclusions are obviously dispersed by the complex purifying process. The phase composition does not change with the refining process and the microstructure of different purifying conditions of sand-cast-T6 GW103K alloy mainly consists of α(Mg)+γ+β' [17,19] (see Fig. 3).

It is known that the purifying ability could be evaluated by comparing the contents of inclusions after refining process. Table 3 shows the statistical volume fractions of nonmetallic inclusions in the alloy. It is obviously that the last three methods significantly reduced the inclusions compared with the unrefined alloy. It should be noted that the volume fraction of inclusions of 1% JDMJ flux with gas bubbling refining is 0.28%, and it is even a little lower than that refined by the conventional 2% JDMJ flux (0.30%). The result indicates that the application of the rotating gas bubbling can substantially improve the efficiency of traditional flux purification by decreasing the amount of JDMJ fluxes at a rate of 50%. However, the sole gas bubbling can only reduce the volume fraction from 0.47% to

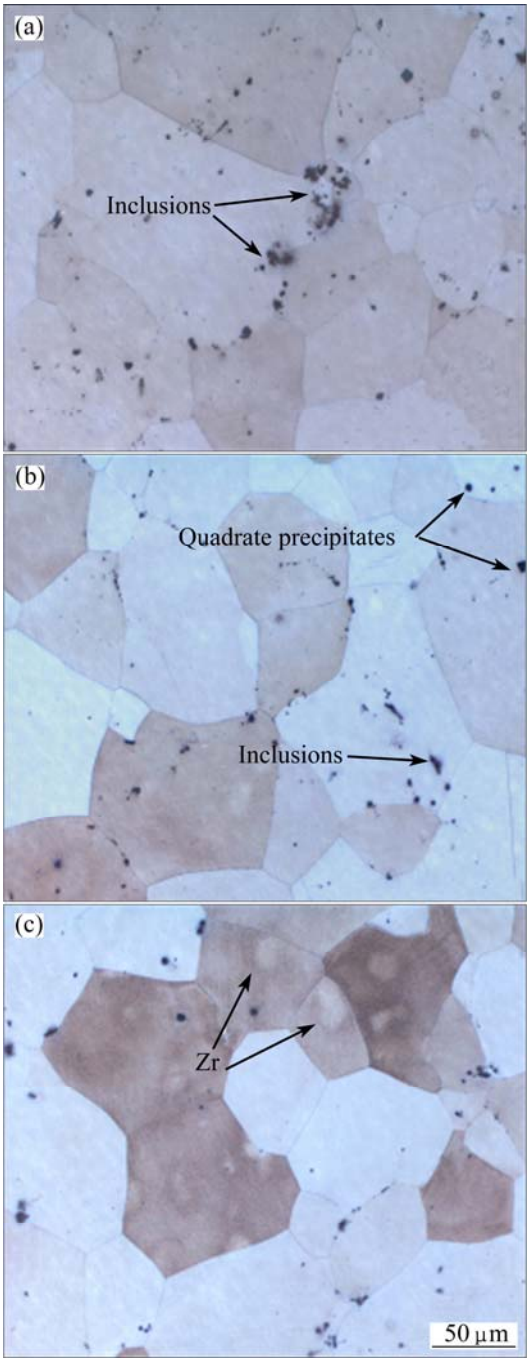

Fig. 4 Microstructures of sand-cast-T6 GW103K alloys purified by different treatments: (a) Unpurified; (b) Gas bubbling; (c) 1% JDMJ flux + gas bubbling

Table 3 Statistical volume fractions of inclusions in GW103K alloys with different treatments

Refining method	Number of fields	Average volume fraction/%
Unpurified	30	0.47
Gas bubbling purifying	30	0.43
2% JDMJ flux purifying	30	0.30
1% JDMJ flux + gas bubbling	30	0.28
2% JDMJ flux + gas bubbling	30	0.27

0.43% and could not achieve the expected results. It is also found that continuously increasing the amount of JDMJ flux to 2% incorporating with gas bubbling slightly improves the inclusions removing ability. On the contrary, excessive addition of flux may lead to flux inclusion (see Fig. 5). Generally, 1% JDMJ flux incorporating with gas bubbling process exhibited the best refining efficiency in terms of inclusions removing.

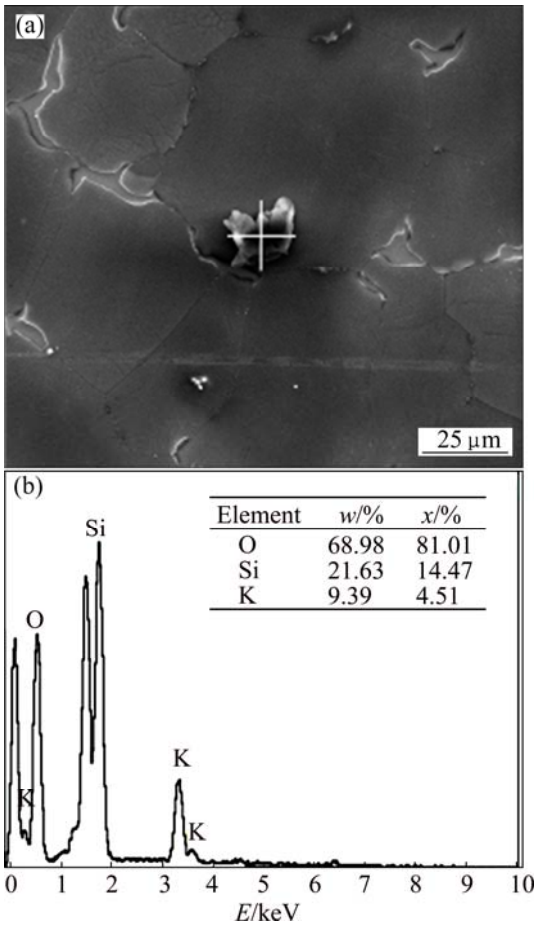

Fig. 5 SEM image (a) and energy dispersive X-ray (EDX) analysis (b) of flux inclusion

3.2 Effect of complex purification treatment on mechanical properties

In the T6 condition, all the eutectic phases which existed in sand-cast condition dissolved into the matrix and only the remaining inclusions play an important role in restricting the comprehensive properties of the GW103K alloys. Thus, the tensile properties of the sand-cast-T6 alloys could somehow reflect the refining effect. Figure 6 show the effect of different purification treatments on the mechanical properties of the sand-cast-T6 alloys. Large improvements of the ultimated tensile strength (UTS) and elongation (EL) are observed through the conventional 2% JDMJ flux refining process compared with the unrefined alloy, which are 297 MPa, 3.7% and 245 MPa, 0.7%, respectively. The UTS and EL reached the maximum 312 MPa and 4.5% when the treatment of 1% JDMJ flux incorporating with rotating gas bubbling was employed. It indicates that the use of melt flux can be decreased by 50% compared with the traditional flux refining process and significantly reduced environmental pollution. Tensile properties improve little, however, with 2% JDMJ flux applied to the complex treatment and more excess flux may induce the appearance of flux inclusions discussed before.

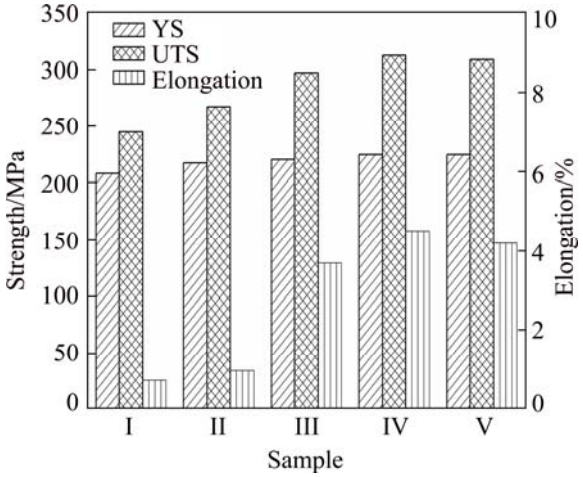

Fig. 6 Tensile properties of sand-cast-T6 GW103K alloys after different purifying methods

In addition, the tensile properties of the sole rotating gas bubbling treated alloy is not so satisfactory (UTS: 267 MPa, EL: 1.0%), showing the refining efficiency is inferior compared with the conventional flux one and the complex treatment one. It should be noted that the UTS and EL of the GW103K alloys exhibit the same rule as the statistical volume fractions of nonmetallic inclusions, and the effect of the non-metallic inclusions on service properties of GW103K alloy was studied comprehensively in Ref. [20]. However, the yield strength (YS) changes little with the refining treatments. This may be because the YS indicates the elastic deformation ability, where the matrix α(Mg) and the precipitated phase after T6 heat treatment play an important role while the elastic deformation progress is not so sensitive to inclusions. Overall, the best combination of mechanical properties can be achieved by 1% JDMJ flux incorporating with gas bubbling treatment.

3.3 Fractography

Figure 7 shows fracture surface SEM micrographs of the tensile specimens of the sand-cast GW103K alloys in various conditions. The whole fracture surface inclines to the loading axis and is close to the plane with maximum shear force. In unrefined alloy (see Fig. 7(a)), the failure surface is composed of fractured eutectics and cleavage planes. Some non-metallic inclusions were

found (Figs. 7(c) and (d)) on the fracture surface of the unrefined specimen which indicates that the micro-crack may partly form from the inclusions and then progress across the grains as cleavage fracture. For the 1% JDMJ flux incorporating with gas bubbling refined alloy, however, cleavage planes are weaker and evident tearing ridges on the alloy fracture surfaces were observed (see Fig. 7(f)). A few dimples were observed as well. Therefore, the plasticity of the GW103K alloy after refining treatment is superior to that of the unrefined one, which is in accordance with the tensile test results. But it is clear that the fracture mechanism is not changed with the refining process which is still quasi-cleavage.

Figure 8 shows the microstructures of fracture surface of GW103K alloy under different treatments in T6 condition. The fracture modes of peak-aging alloys are all quasi-cleavage fractures. The unrefined one is composed of massive cleavage planes and grain boundaries while less cleavage planes, more tear ridges comparatively are found in the complex purified

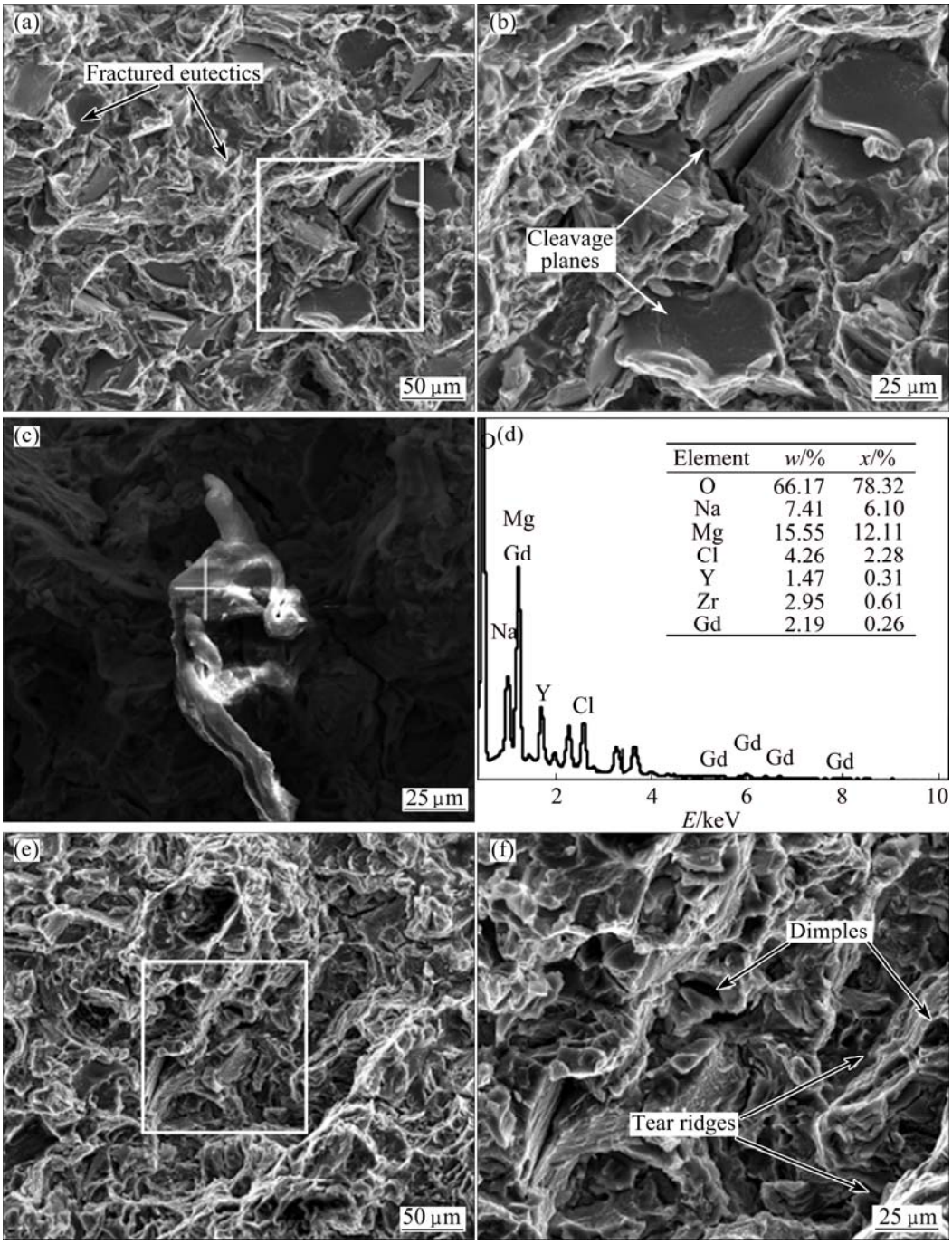

Fig. 7 Typical fractographies of tensile specimens of sand-cast alloys in different conditions: (a) Unpurified; (b) Magnified view of central region in (a); (c) SEM photograph; (d) EDS analysis of nonmetallic inclusions in as-cast tensile specimens; (e) 1% JDMJ flux + gas bubbling; (f) Magnified view of central region in (e)

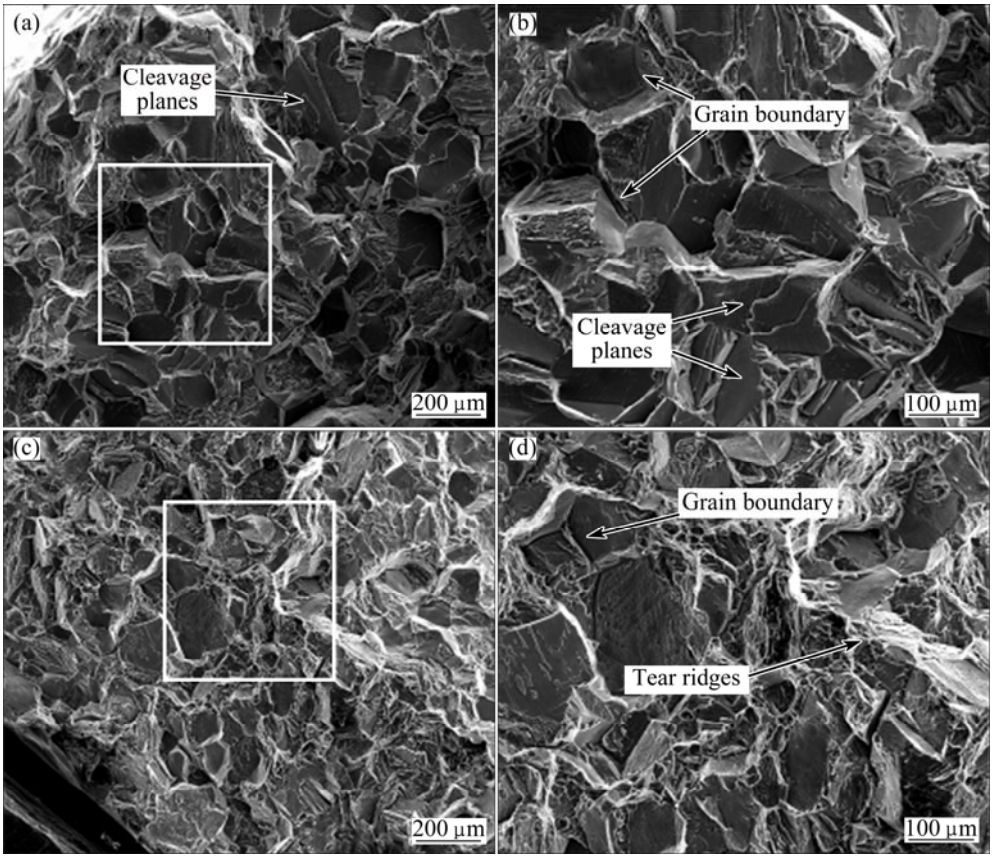

Fig. 8 Typical fractographs of tensile specimens of sand-cast-T6 alloys in different conditions: (a) Unpurified; (b) Magnified view of central region in (a); (c) 1% JDMJ flux + gas bubbling; (d) Magnified view of the central region in (c)

specimen. It explains the plasticity improvement with the progress of 1% JDMJ flux incorporating with gas bubbling treatment. In general, the refining process would not change the fracture mechanism but it has a certain effect on the fracture pattern no matter in the sand-cast or sand-cast-T6 condition.

The optical microstructures of ruptured samples perpendicular to the fracture surface are shown in Figs. 9 and 10. The GW103K alloys show different secondary crack morphologies in different conditions. Apparent transgranular cracks are observed in both sand-cast and sand-cast-T6 unrefined alloys (Figs. 9(a) and 10(a)), which indicates that fracture mode is mainly transgranular fracture confirmed by SEM analysis before. In the sand-cast refining specimen, secondary cracks along the grain boundary and at grain interior are observed (Fig. 9(d)). After T6 heat treatment, however, less secondary crack is found (Fig. 10(c)). It may have close relation with the dissolving of eutectic phases, which have a stronger effect on the mechanical properties than inclusions discussed before.

4 Discussion

The employment of rotating gas bubble stirring can significantly improve the efficiency of the conventional flux purification for magnesium alloys. Generally, the mechanism could be illustrated by the following discussion.

On one hand, it is known that the inclusion transmission is one of the most restricted links of flux refining process. And the appropriate continuous stirring in this method (150 r/min, 10 min) can help the inclusions transfer near the interface between magnesium melt and JDMJ flux rapidly. Hydromechanics retardation (named as H) then appeared as shown in Fig. 11, however, before the inclusions transit to the interface between melt and flux. Only when the distance between inclusions and the interface is close enough, the inclusions can be captured by fluxes. So, the refining efficiency partly depends on the key process of inclusions breaking through the melt layer which separates inclusions and fluxes.

The situation is similar to the inclusion movement in Al melt [21], where the replacing speed can be illustrated as

$$u=\frac{\mathrm{d}(1/H^2)}{\mathrm{d}t}=\frac{F}{3D_{\mathrm{k}}{}^2\eta_{\mathrm{melt}}} \tag{1}$$

$$F=\sigma_{\text{melt-flux}}/r_{\mathrm{k}} \tag{2}$$

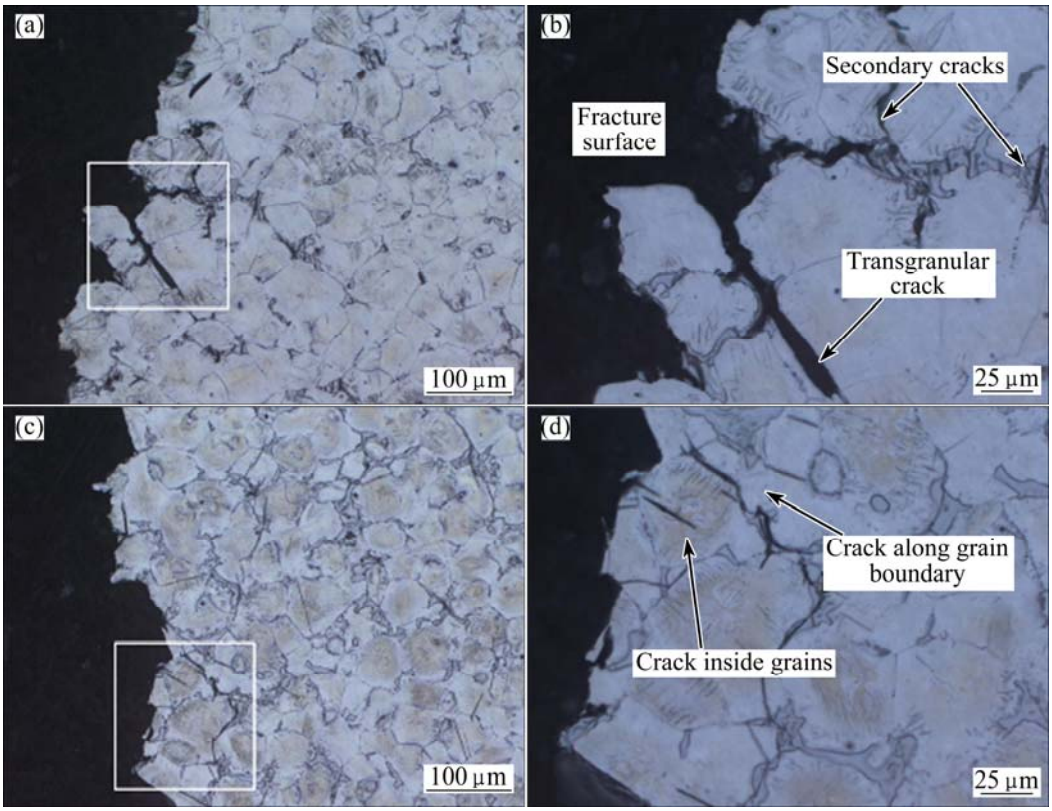

Fig. 9 Optical images of longitudinal section of fracture surface of sand-cast alloys in different conditions: (a) Unpurified; (b) Magnified view of central region in (a); (c) 1% JDMJ flux + gas bubbling; (d) Magnified view of central region in (c)

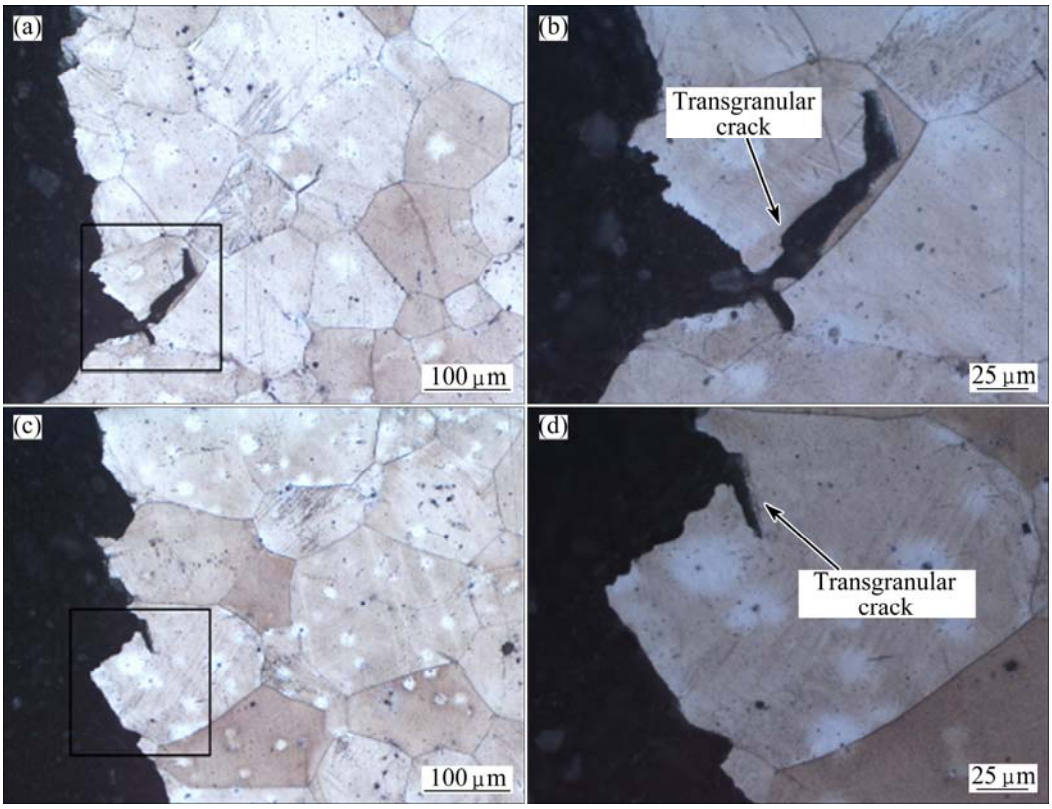

Fig. 10 Optical images of longitudinal section of fracture surface of sand-cast-T6 alloys in different conditions: (a) Unpurified; (b) Magnified view of central region in (a); (c) 1% JDMJ flux + gas bubbling; (d) Magnified view of central region in (c)

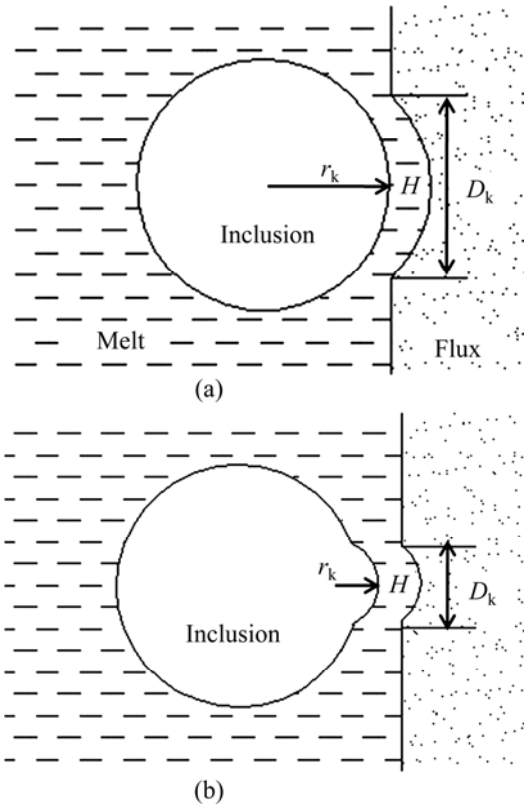

Fig. 11 Schematic diagram showing behaviour of inclusions near interface between melt and flux: (a) Inclusion with smooth surface; (b) Inclusion with sharp angle shape

Then,

$$u=\frac{\sigma_{\text{melt-flux}}/r_{\text{k}}}{3D_{\text{k}}^2\eta_{\text{metal}}} \tag{3}$$

where H is hydromechanics retardation; F is the remaining pressure of melt-flux contact zone; $\sigma_{\text{melt-flux}}$ is the interface tension between GW103K alloy melt and JDMJ flux; r_{k} is the curvature radius of the interface layer and η_{melt} is the viscosity of alloy melt.

The energy which supports this transmission process rooted in the kinetic energy of the inclusions near the interface layer, and it can be expressed as

$$E_{\text{k}}=\frac{1}{2}mv_{\text{v}}^2 \tag{4}$$

where m is the mass of inclusions; v_{v} is vertical velocity component of inclusions.

While the rotating treatment was employed, the inclusion particles may break into debris which refers to the condition as shown in Fig. 11(b). Then, ascribing to the function mixed of the mechanical agitation and the collision with the inert gas, the velocity value of these inclusions increases significantly. Most huge inclusions will be separated into fast-speed small sharp angle shape ones, which means smaller r_{k}, D_{k} and larger v_{v}. In this case, according to Eqs. (3) and (4), it can be concluded that the speed of inclusions u during the overcoming hydromechanics retardation period increases sharply, and the energy E_{k} is big enough to satisfy this process. This partly explains the efficiency improvement in the complex purification.

On the other hand, the gas bubbling itself has some refining ability, too. It is known that most inclusions can be wetted by fluxes, and settle to the bottom of the crucible. But very small inclusions cannot be captured by fluxes due to its insignificant E_{k}. But these inclusions can be wetted by the Ar gas, and then float up. The floating process can be explained by the following analysis.

When the inclusions adhere to the spraying gas once they touch the gas and the gas around the inclusions [22], the stress condition of the single inclusion in the Mg melt can be shown as Fig. 12. According to stress equilibrium relationship,

$$F_{\text{b}}+F_{\text{f}}=F_{\text{w}} \tag{5}$$

then,

$$(V_{\text{inclusion}}\rho_{\text{inclusion}}+V_{\text{gas}}\rho_{\text{gas}})g=V\rho_{\text{metal}}g+\frac{1}{2}C_{\text{d}}\rho_{\text{metal}}Av^2 \tag{6}$$

Take the spherical particle as an example, then,

$$V_{\text{inclusion}}=\frac{4}{3}\pi r_{\text{inclusion}}^3 \tag{7}$$

$$V=\frac{4}{3}\pi r^3 \tag{8}$$

$$V_{\text{gas}}=V-V_{\text{inclusion}}\quad (r>r_{\text{inclusion}}) \tag{9}$$

$$A=\pi r^2,\quad C_{\text{d}}=\frac{24}{Re},\quad Re=\frac{2rv\rho_{\text{metal}}}{\eta_{\text{metal}}} \tag{10}$$

It can be deduced [22],

$$v=\frac{2\text{g}}{9\eta_{\text{metal}}r}[r_{\text{inclusion}}^3(\rho_{\text{incusion}}-\rho_{\text{gas}})+r^3(\rho_{\text{gas}}-\rho_{\text{metal}})] \tag{11}$$

where v is the particle settling velocity; g is the gravity acceleration; η_{metal} is the viscosity coefficient; $r_{\text{inclusion}}$ is the inclusion particle radius; r is the radius of aggregate of inclusion absorbing gas; $\rho_{\text{inclusion}}$ is the inclusion density; ρ_{gas} is the gas density; ρ_{metal} is the metal density. $V_{\text{inclusion}}$ is the inclusion particle volume; V is the volume of aggregate of inclusion absorbing gas; V_{gas} is the gas particle volume; C_{d} is the drag coefficient; A is the projected area of a particle; Re is the Reynolds number.

As the assumption made before, after Ar gas spraying into the Mg melt, the inclusion particles are wetted by gas, then r increases. The very small inclusions have the very small radius $r_{\text{inclusion}}$, and r

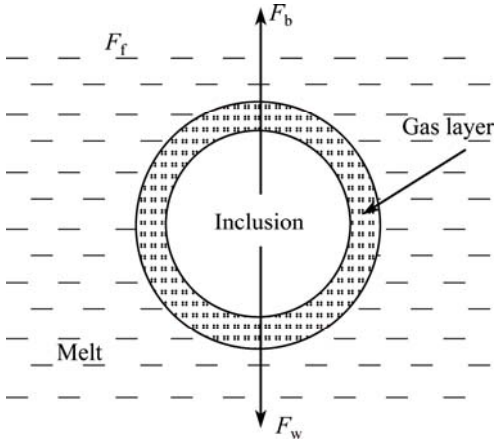

Fig. 12 Schematic diagram of inclusion particle with gas covered (F_b is the particle buoyant force; F_w is the particle gravity force; F_f is the viscosity resistance)

increases with the gas bubbling process. In this case, according to Eq. (11), $\rho_{inclusion} - \rho_{gas}$ is positive while $\rho_{gas} - \rho_{metal}$ is negative. If the $r_{inclusion}$ is small enough and the r is big enough, the v result might be negative, which means these inclusions will not settle, but float up. In addition, the degassing ability of gas bubbling also helps to improve the purity of alloy melt. It should be noted that as the inclusions discussed in this case is the minority, the floating process is not so active. And it explains why the refining treatment of sole rotating gas bubble stirring is not so efficient.

5 Conclusions

1) The phase composition does not change with different refining treatments, the microstructure of the alloy still consists of α(Mg)+Mg_{24}(Gd, Y)$_5$ and α(Mg)+γ+β' phase for sand-cast and sand-cast-T6 conditions, respectively.

2) Combined rotating gas bubble stirring with flux is an effective new method in refining Mg−10Gd−3Y−0.5Zr alloy. While 1% JDMJ flux incorporating with rotating gas bubbling refining method is employed, the volume fractions of nonmetallic inclusions in the unrefined alloy can be reduced significantly from 0.47% to 0.28%, where clean melt can be achieved. Correspondingly, the UTS and the EL reach 312 MPa, 4.5% respectively compared with 245 MPa, 0.7% for the unrefined one.

3) The employment of gas bubbling into the conventional flux refining can significantly improve the purifying efficiency by reducing the amount of JDMJ flux from 2% to 1% without decreasing the refining ability. However, the sole gas bubbling refining ability is inferior compared with that under the complex treatment and the conventional flux one.

4) The refining process would not change the fracture mechanism but it has a certain effect on the fracture pattern no matter in the sand-cast or sand-cast-T6 condition.

References

[1] BAE D H, KIM S H, KIM D H, KIM W T. Deformation behavior of Mg−Zn−Y alloys reinforced by icosahedral quasicrystalline particles [J]. Acta Materialia, 2002, 50(9): 2343−2356.

[2] LIU W C, DONG J, ZHANG P, YAO Z Y, ZHAI C Q, DING W J. High cycle fatigue behavior of as-extruded ZK60 magnesium alloy [J]. Journal of Materials Science, 2009, 44(11): 2916−2924.

[3] FEYERABEND F, FISCHER J, HOLTZ J, WITTE F, WILLUMEIT R, DRÜCKER H, VOGT C, HORT N. Evaluation of short-term effects of rare earth and other elements used in magnesium alloys on primary cells and cell lines [J]. Acta Biomaterialia, 2010, 6(5): 1834−1842.

[4] ANYANWU I A, KAMADO S, KOJIMA Y. Aging characteristics and high temperature tensile properties of Mg−Gd−Y−Zr alloys [J]. Materials Transactions, 2001, 42: 1206−1211.

[5] MIRZA F A, CHEN D L, LI D J, ZENG X Q. Effect of rare earth elements on deformation behavior of an extruded Mg−10Gd−3Y−0.5Zr alloy during compression [J]. Materials and Design, 2013, 46: 411−418.

[6] HE Shang-ming, ZENG Xiao-qin, PENG Li-ming, GAO Xiao-qin, NIE Jian-feng, DING Wen-jiang. Precipitation in a Mg−10Gd−3Y−0.4Zr (wt. %) alloy during isothermal aging at 250 °C [J]. Journal of Alloys and Compounds, 2006, 421(1−2): 309−313.

[7] CHANG Jian-wen, GUO Xing-wu, HE Shang-ming, FU Peng-huai, PENG Li-ming, DING Wen-jiang. Investigation of the corrosion for Mg−xGd−3Y−0.4Zr (x=6%, 8%, 10%, 12%, mass fraction) alloys in a peak-aged condition [J]. Corrosion Science, 2008, 50: 166−177.

[8] WANG Jun, MENG Jian, ZHANG De-ping, TANG Ding-xiang. Effect of Y for enhanced age hardening response and mechanical properties of Mg−Gd−Y−Zr alloys [J]. Materials Science and Engineering A, 2007, 456: 78−84.

[9] HONMA T, OHKUBO T, KAMADO S, HONO K. Effect of Zn on age hardening and elongation in Mg−2.0Gd−1.2Y−0.2 Zr alloy [J]. Acta Materialia, 2007, 55: 4137−4150.

[10] DU Wen-bo, WU Yu-feng, NIE Zuo-ren, SU Xue-kuan, ZUO Tie-yong. Effect of rare earth and alkaline earth on magnesium alloys and their applications status [J]. Rare Metal Materials and Engineering, 2006, 35(9): 1345−1349.

[11] GAO Hong-tao, WU Guo-hua, DING Wen-jiang, ZHU Yan-ping. Purifying effects of new flux on magnesium alloy [J]. Transactions of Nonferrous Metals Society of China, 2004, 14(3): 530−536.

[12] WU Guo-hua, XIE Min, ZHAI Chun-quan, ZENG Xiao-qin, ZHU Yan-ping, DING Wen-jiang. Purification technology of AZ91 magnesium alloy wastes [J]. Transactions of Nonferrous Metals Society of China, 2003, 13(6): 1260−1264.

[13] WU Rui-zhi, QU Zhi-kun, SUN Bao-de, SHU Da. Effects of spray degassing parameters on hydrogen content and properties of commercial purity aluminum [J]. Materials Science and Engineering A, 2007, 456: 386−390.

[14] ZHAO Lei, PAN Ye, LIAO Heng-cheng, WANG Qi-gui. Degassing of aluminum alloys during re-melting [J]. Materials Letters, 2012, 66(1): 328−331.

[15] LUO A A. Magnesium casting technology for structural applications [J]. Journal of Magnesium and Alloys, 2013, 1(1): 2−22.

[16] XU Jia, WU Guo-hua, LIU Wen-cai, ZHANG Yang, DING Wen-jiang. Effects of rotating gas bubble stirring treatment on the microstructures of semi-solid AZ91−2Ca alloy [J]. Journal of

Magnesium and Alloys, 2013, 1(3): 217−223.
[17] HE Shang-ming, ZENG Xiao-qin, PENG Li-ming, GAO Xiang, NIE Jian-feng, DING Wen-jiang. Microstructure and strengthening mechanism of high strength Mg−10Gd−2Y−0.5Zr alloy [J]. Journal of Alloys and Compounds, 2007, 427: 316−323.
[18] WANG Wei, HUANG Yu-guang, WU Guo-hua, WANG Qu-dong, SUN Ming, DING Wen-jiang. Influence of flux containing YCl3 additions on purifying effectiveness and properties of Mg−10Gd−3Y−0.5Zr alloy [J]. Journal of Alloys and Compounds, 2009, 480(2): 386−391.
[19] WANG Qi-long, WU Guo-hua, HOU Zheng-quan, CHEN Bin, ZHENG Yun, DING Wen-jiang. A comparative study of Mg−Gd−Y−Zr alloy cast by metal mould and sand mould [J]. China Foundry, 2010, 7(1): 6−12.
[20] LIANG Min-jie, WU Guo-hua, DING Wen-jiang, WANG Wei. Effect of inclusion on service properties of GW103K magnesium alloy [J]. Transactions of Nonferrous Metals Society of China, 2011, 21(4): 717−724.
[21] LI Pei-jie, GUO Jing-seng, JIA Jun, LI Qing-chun, Thermodynamical and kinetic analysis of flux refining in Al melt [J]. Material Science & Technology, 1995, 3(3): 82−86.
[22] WU Guo-hua, DAI Ji-chun, SUN Ming, DING Wen-jiang. Non-flux purification behavior of AZ91 magnesium alloy [J]. Transactions of Nonferrous Metals Society of China, 2010, 20(11): 2037−2045.

熔体复合净化处理对砂型铸造 Mg−10Gd−3Y−0.5Zr 镁合金显微组织和力学性能的影响

梅 俊[1]，刘文才[1,2]，吴国华[1]，张 杨[1]，张逸韬[1]，洪毅恺[1]，张若曦[1]，肖 旅[3]，丁文江[1]

1. 上海交通大学 轻合金精密成型国家工程研究中心，金属基复合材料国家重点实验室，上海 200240；
2. 上海轻合金精密成型国家工程研究中心有限公司，上海 201615；
3. 上海航天精密机械研究所，上海 201600

摘 要：采用金相分析、SEM 和拉伸试验等试验方法分析和测试砂型铸造 Mg−10Gd−3Y−0.5Zr 镁合金熔体复合净化处理(旋转喷吹氩气结合熔剂净化)后的显微组织和室温力学性能，讨论复合处理方法净化机理。结果表明，该复合处理可以显著提高熔体质量，大幅度提高合金力学性能。熔体经过复合净化处理后，合金夹杂物体积分数从 0.47%降低到 0.28%，抗拉强度和伸长率从 245 MPa 和 0.7%分别提高至 312 MPa 和 4.5%。1%熔剂复合旋转喷吹气体净化效果甚至更优于传统的 2%熔剂净化效果，熔剂的使用量减少了 50%，显著提高了净化效率，并缓和了熔剂净化带来的环境污染问题。

关键词：镁合金；砂型铸造；净化；熔体复合处理；力学性能

(Edited by Yun-bin HE)